



OPEN

1,2,3-triazole and chiral Schiff base hybrids as potential anticancer agents: DFT, molecular docking and ADME studies

Yonas Belay^{1✉}, Alfred Muller¹, Fanikie S. Mokoena¹, Adedapo S. Adeyinka¹, Lesetja R. Motadi² & Abel K. Oyebamiji³

A series of novel 1,2,3-triazole and chiral Schiff base hybrids 2–6 were synthesized by Schiff base condensation reaction from pre-prepared parent component of the hybrids (1,2,3-triazole 1) and series of primary chiral amines and their chemical structure were confirmed using NMR and FTIR spectroscopies, and CHN elemental analysis. Compounds 1–6 were evaluated for their anticancer activity against two cancer PC3 (prostate) and A375 (skin) and MRC-5 (healthy) cell lines by Almar Blue assay method. The compounds exhibited significant cytotoxicity against the tested cancer cell lines. Among the tested compounds 3 and 6 showed very good activity for the inhibition of the cancer cell lines and low toxicity for the healthy cell lines. All the compounds exhibited high binding affinity for Androgen receptor modulators (PDB ID: 5t8e) and Human MIA (PDB ID: 1i1j) inhibitors compared to the reference anticancer drug (cisplatin). Structure activity relationships (SARs) of the tested compounds is in good agreement with DFT and molecular docking studies. The compounds exhibited desirable physicochemical properties for drug likeness.

Keywords Cancer, Hybrid drugs, 1,2,3-triazole, Chiral Schiff bases, Molecular docking, ADME

Cancer is a complex disease, and it ranks as the second leading cause of mortality worldwide^{1,2}. It was estimated that 19.3 million new cases of cancer and almost 10.0 million cancer-related deaths were reported in 2020³. According to global demographic trends, 420 million new cancer cases are expected annually by 2025⁴. The current available drugs that have been employed for cancer treatment are not effective due to lack of efficacy and poor selectivity, the latter of which could lead to adverse side effects⁵. In addition, the emergence of drug resistance has hampered the effectiveness of these drugs in the clinic⁶. Thus, there is an urgent need to develop effective, safe, and selective anticancer agents with enhanced properties that could overcome current limitations in chemotherapy treatment. A combination of two or more pharmacophores or synthesis of hybrid molecules constituting two or more bioactive entities could be a viable solution to fight drug resistance in cancer cells^{7–10}. Hybrid drugs can extend the spectrum of biological activity, enhance the potency, overcome drug resistance, reduce side effects, and improve pharmacokinetic, pharmacodynamic as well as physicochemical profiles^{11–15}. Literature reports indicated that several hybrids have been synthesized and are under different phase clinical trials for the treatment of various diseases including those caused by drug-resistant organisms, revealing hybridization is a useful strategy to develop novel anticancer drugs¹⁶.

1,2,3-Triazoles are one of the most important classes of nitrogen-containing heterocycles and can form various non-covalent interactions such as hydrophobic interactions, hydrogen bonds, van der Waals forces and dipole–dipole bonds with various enzymes, proteins, and receptors^{17,18}. Therefore, triazole derivatives have attracted considerable attention due to their chemotherapeutic values such as antibacterial^{11,19,20}, antimalarial^{21,22}, antiviral²³, antifungal²⁴, antitubercular^{25,26}, and anticancer activities^{27–31}. Reported examples of 1,2,3-triazole-containing compounds that exhibited anticancer activity are Cefatrizine derivative, carboxyamido-triazoles, azido- β -lactam, amprenavir derivative, 1,2,3-triazole-dithiocarbamate-urea hybrid and N-((1-benzyl-1H-1,2,3-triazole-4-yl)methyl)arylamid derivative. Cefatrizine and Carboxyamido-triazoles (Fig. 1) have already been used

¹Department of Chemical Sciences, University of Johannesburg, P.O. Box 524, Auckland Park 2006, South Africa. ²Department of Biochemistry, University of Johannesburg, P.O. Box 524, Auckland Park 2006, South Africa. ³Industrial Chemistry Programme, Bowen University, PMB 284, Iwo, Osun State, Nigeria. ✉email: yhbelay@yahoo.com

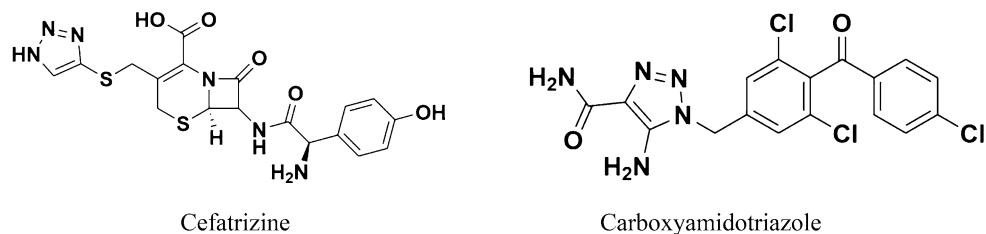


Figure 1. Reported 1,2,3-triazole containing compounds which are under clinical evaluation for cancer treatment.

in clinics or are under clinical evaluation for cancer treatment, revealing their potential as putative anticancer drugs³².

Schiff bases are organic compounds formed by the condensation reaction of aldehydes or ketones with primary amines³⁴. The presence of a lone pair of electrons of the nitrogen atoms' sp^2 hybridized orbital in the azomethine group is critical for their chemical and biological activities³⁵ that render these as viable candidates for the anticancer properties of Schiff bases^{36–38} and their metal complexes^{39–41}.

Chiral drugs are at the forefront of pharmaceutical drug research as introduction of chirality not only enforces stereo-selective specific drug interaction but also promotes the formation of active compounds with therapeutic benefits as most of the biotargets viz., DNA (the primary intracellular target) is chiral in nature⁴². Being inherently chiral, the double-stranded helical DNA can interact with chiral substrate resulting in different enantiomeric structures in a stereospecific way leading to different DNA-substrate adduct profiles⁴³. On the other hand, the presence of planar molecules substituted with free functional groups like alcoholic, phenolate, amine, oxime, etc. might have a superior chemical binding profile with DNA molecules⁴³. Inspired by the reported anticancer properties of 1,2,3-triazole, Schiff bases and chiral compounds and as a continuation of our research on the synthesis of 1,2,3-triazole hybrid compounds for medicinal applications⁴⁴ herein, we report the synthesis of 1,2,3-triazole and chiral Schiff base hybrids and evaluation of their anticancer activities, DFT, molecular docking and druglikeness studies.

Results and discussions

The one component of the hybrids, 1,2,3-triazole **1** was Previously synthesized through multistep synthesis by copper catalyzed click chemistry reaction of preprepared 2-(prop-2-yn-1-yloxy) benzaldehyde with azido-benzene. The structure of the compound was confirmed by ¹H NMR spectroscopy. The disappearance of the signal for the terminal alkyne proton from 2-(prop-2-yn-1-yloxy) benzaldehyde at 2.55 ppm and appearance of the diagnostic low field singlet signal for the triazole ring proton at 8.08 ppm established the structure of 2-((1-phenyl-1H-1,2,3-triazol-4-yl)methoxy)benzaldehyde (**1**) (Fig. S1)⁴⁴. Other characterization techniques such as FTIR, mass spectrometry and CHN elemental analysis were performed which established the formation of **1** (see experimental procedure). Compound **1** was exposed to different solvents for obtaining single crystals suitable for single crystal X-ray diffraction. Single crystals of **1** was obtained after one week from ethanol by slow evaporation. Single crystal analysis (Fig. 2) revealed that **1** crystallized in triclinic space group *P* $\bar{1}$. Details of the X-ray crystallographic data for the compound are given in Table 1 and rest of the structural parameters (bond lengths/angles and hydrogen parameters) are provided in the supplementary documents (Table S1).

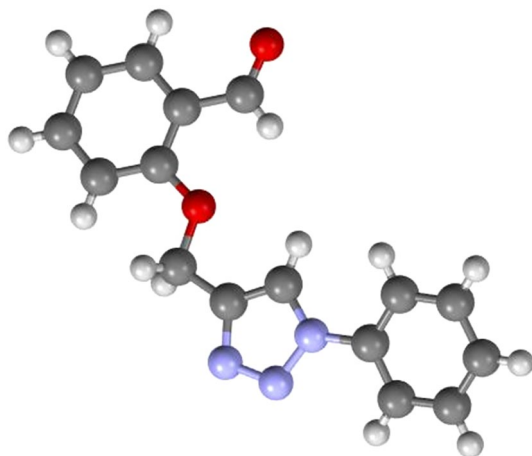


Figure 2. Crystal structure of compound **1**.

Identification code	CCDC 2297996
Empirical formula	C ₃₄ H ₂₈ N ₄ O ₄
Formula weight	556.60
Temperature	173 (2) K
Wavelength	0.71073 Å
Crystal system	Triclinic
Space group	P $\bar{1}$
a/Å	4.4158 (14)
b/Å	15.086 (5)
c/Å	19.788 (7)
α /°	83.221 (11)
β /°	90
γ /°	90
Volume	1309.0(8) Å ³
Z	2
Density (calculated)	1.412 Mg/m ³
Absorption coefficient	0.094 mm ⁻¹
F(000)	584
Crystal size	0.300 × 0.110 × 0.100 mm ³
Theta range for data collection	1.036 to 28.641°
Index ranges	- 5 ≤ h ≤ 5, - 20 ≤ k ≤ 19, - 26 ≤ l ≤ 26
Reflections collected	20,610
Independent reflections	6372 [R(int) = 0.1454]
Completeness to theta = 25.242°	98.9%
Refinement method	Full-matrix least-squares on F ²
Data/restraints/parameters	6372/0/379
Goodness-of-fit on F ²	0.869
Final R indices [I > 2sigma (I)]	R1 = 0.0734, wR2 = 0.1556
R indices (all data)	R1 = 0.2329, wR2 = 0.2259
Extinction coefficient	n/a
Largest diff. peak and hole	0.252 and - 0.296 e.Å ⁻³

Table 1. Crystal data and structure refinement for compound **1**.

Synthesis of hybrids of 1,2,3-triazole and chiral Schiff bases (2–6)

The reaction for the synthesis of the hybrid compounds is shown in Fig. 3. The reaction was performed by Schiff base condensation of the preprepared triazole **1** with primary chiral amines (*D*-glutamic acid, *L*-tryptophan, *L*-tyrosine and *L*-histidine) and an enantiomer Phenylalanine ethyl ester hydrochloride in the presence of sodium hydroxide as a base and provided the proposed hybrids of 1,2,3-triazole and chiral Schiff bases (2–6). The structures of the compounds were characterized using NMR and FTIR spectroscopy (see supplementary material Figs. S1–S14) as well as CHN elemental analysis.

The ¹H NMR spectra of compounds (2–6) showed characteristic signals of the protons corresponding to the imine moiety between 9.02 and 8.06 ppm and the 1,2,3-triazole group between 8.92 and 7.92 ppm. The appearance of characteristic high field singlet signal between 5.55 and 2.68 ppm and between 5.26 and 2.63 ppm, respectively was attributed to the methine and methylene protons of the chiral amino acids. The appearance of characteristic high field singlet signal between 5.44 and 5.21 ppm was attributed to the methylene protons attached to the phenolic and 1,2,3-triazole groups. Moreover, the appearance of characteristic low field broad singlet signals in compounds **2** and **6** between 10.41 and 10.34 ppm and at 10.42 ppm, respectively was assigned to the hydroxyl protons of the chiral amino acids (*D*-glutamic acid and phenyl alanine). The broad singlet signal at 10.68 ppm in compound **3** is evident for the NH proton of the chiral amino acid (*L*-tryptophan). The absence of characteristic low field broad singlet signal in compounds **3**, **4**, and **5** is due to the deprotonation of the hydroxyl protons of the chiral amino acids by sodium hydroxide. In ¹³C NMR spectra, the presence of characteristic signals between 160.4 and 157.0 ppm correspond to the imine carbon (C=N). The presence of characteristic signals between 144.3 and 143.3 ppm for N–C=CH and between 120.3 and 120.1 ppm for N–C=CH, correspond to the 1,2,3-triazole carbons. The carbonyl carbon is evident between 192.1 and 174.8 ppm. The characteristic signals between 98.6 and 59.7 ppm for N–CH–CH₂ and between 55.5 and 30.1 ppm for N–CH–CH₂, respectively correspond to the methine and methylene carbons of the chiral amino acids. The characteristic signal for the methylene carbon (CH₂OAr) is attributed between 61.9 and 56.6 ppm. The molecular structures of compounds 2–6 were also characterized by FTIR spectroscopy (Fig. S14). The FTIR absorption spectra of compounds showed characteristic bands of the imine moiety between 1595 and 1598 cm⁻¹ corresponding to the stretching of C=N bond. In compound **2**, the broad absorption band at ca. 3479 cm⁻¹ and the strong absorption peak at 1667 cm⁻¹

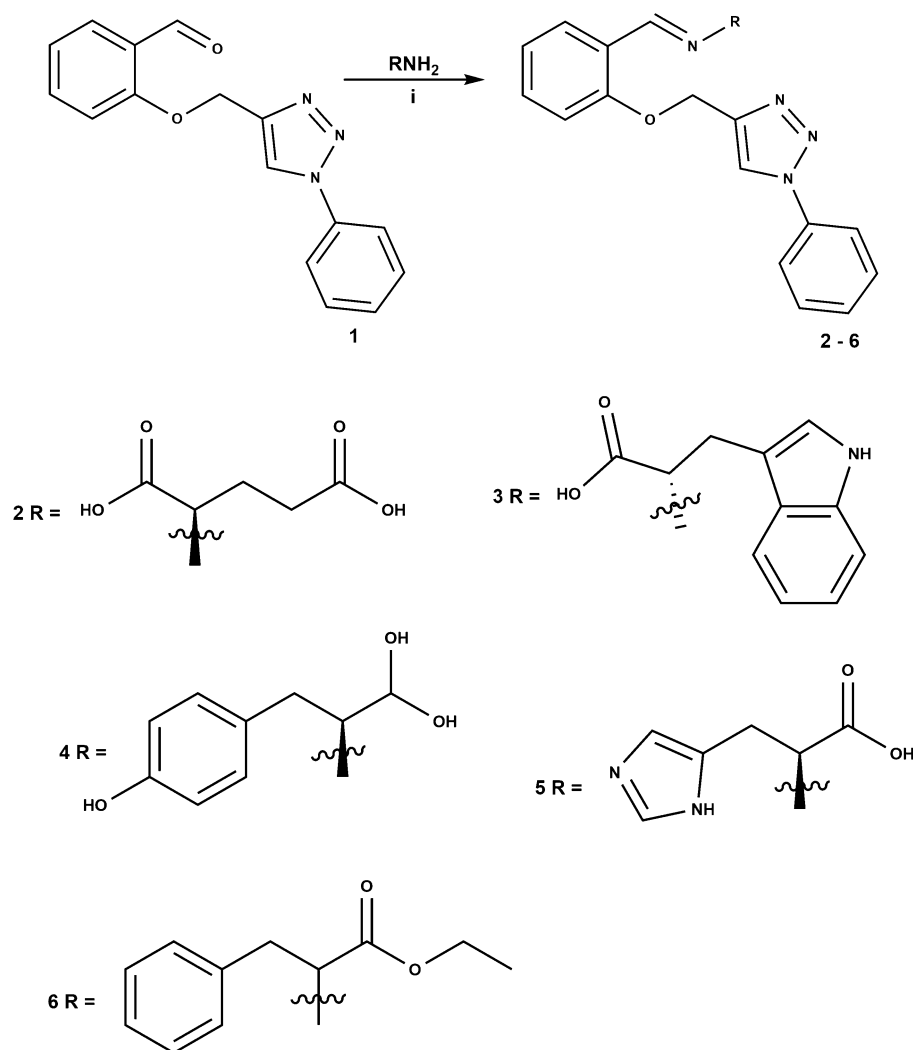


Figure 3. Synthesis of the hybrids of 1,2,3-triazole and chiral Schiff bases. (i) NaOH, MeOH, 80 °C, 1 h.

were attributed to the ν (OH stretch) and ν (C=O stretch) of the glutamic acid, respectively. In compound 6, the broad absorption band at *ca.* 3353 cm^{-1} was attributed to the ν (OH stretch) of the phenyl alanine. The absence of characteristic broad absorption band for ν (OH stretch) in the FTIR spectra of compounds 3, 4, and 5 is evident for the deprotonation of the hydroxyl protons of the chiral amino acids by sodium hydroxide. Summary of ¹H and ¹³C chemical shift of azomethine moiety, IR absorption of C=N and CHN elemental analysis results for compounds 2–6 is shown in Table 2.

Anticancer study

The previously synthesized parent component of the hybrids (1,2,3-triazole) 1 and hybrids of 2–6 were evaluated for their anticancer activities against PC3 (prostate) and A375 (skin) cancer and MRC5 (healthy lung) cell lines with various concentrations of 100, 75, 50, 25, 15 and 5 $\mu\text{g}/\text{mL}$. The test results for IC₅₀ values are presented in Table 3. Cisplatin was used as standard, and it showed an IC₅₀ value of 30.11 $\mu\text{g}/\text{mL}$ for the cancer cells and an IC₅₀ value of 60.34 $\mu\text{g}/\text{mL}$ for MRC5 (normal) cell. All the compounds showed lower activity for the inhibition of the PC3 cancer cell lines with IC₅₀ value in the range of 40.46–75.05 $\mu\text{g}/\text{mL}$ compared to the standard cisplatin with IC₅₀ value of 30.11 $\mu\text{g}/\text{mL}$. Among the tested compounds 3 and 6 exhibited very good activity with IC₅₀ values of 40.46 and 45.00 $\mu\text{g}/\text{mL}$, respectively. Compounds 2, 4 and 5 showed moderate activity and 1 showed lower activity with IC₅₀ value of 75.05 $\mu\text{g}/\text{mL}$ for the proliferation of the PC3 cancer cell lines. For the inhibition of A375 cancer cell lines, most of the compounds exhibited anticancer activity with IC₅₀ values in the range of 21.86–40.37 $\mu\text{g}/\text{mL}$ comparable to the standard cisplatin with IC₅₀ value of 30.11 $\mu\text{g}/\text{mL}$. Compounds 3–6 showed better activity than the standard cisplatin with IC₅₀ values in the range of 21.86–28.94 $\mu\text{g}/\text{mL}$, while 1 and 2 exhibited very good activity at the concentration of 36.12–40.37 $\mu\text{g}/\text{mL}$. Compounds 1–6 were also evaluated for their cytotoxicity against MRC5 normal cells. Surprisingly, all the compounds exhibited less toxicity with

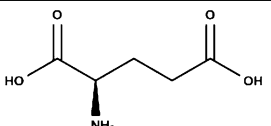
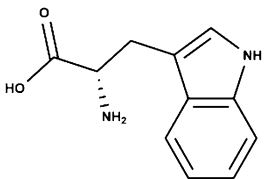
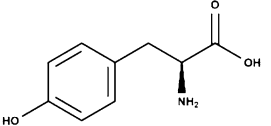
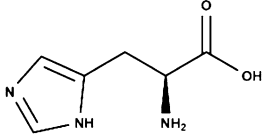
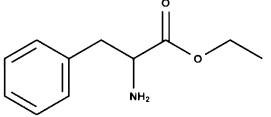
R-NH ₂	Product	¹ H NMR H-C=N (ppm)	¹³ C NMR C=N (ppm)	IR ν (cm ⁻¹) C=N	CHN: anal. calcd (found) %		
					C	H	N
	2	9.00	160.4	1595	61.76 (61.08)	4.94 (5.32)	13.72 (13.14)
	3	8.89	157.0	1595	66.52 (66.13)	4.55 (4.96)	14.37 (13.98)
	4	8.07	157.3	1598	61.73 (61.34)	4.14 (4.52)	11.52 (10.85)
	5	8.06	157.1	1584	60.27 (59.61)	4.37 (4.79)	19.17 (18.58)
	6	9.02	160.3	1578	70.41 (69.75)	5.20 (5.59)	13.14 (12.52)

Table 2. Synthesized hybrids of 1,2,3-triazole and chiral Schiff bases (2–6), ¹H and ¹³C NMR chemical shifts of azomethine moiety, IR absorption of C=N and their CHN elemental analysis.

Compound	Cytotoxicity (IC ₅₀ , µg/mL)		
	PC3	A375	MRC5
1	75.05 ± 1.82	40.37 ± 1.03	76.90 ± 1.87
2	60.59 ± 1.42	36.12 ± 0.87	85.33 ± 2.27
3	40.46 ± 1.06	21.86 ± 0.52	86.40 ± 2.64
4	55.69 ± 1.28	24.83 ± 0.61	88.40 ± 2.38
5	60.53 ± 1.34	28.94 ± 0.65	79.42 ± 2.71
6	45.00 ± 1.12	24.18 ± 0.57	93.07 ± 2.42
Cisplatin	30.11 ± 0.76	30.11 ± 0.69	60.34 ± 1.23

Table 3. IC₅₀ values of compounds 1–6 screened for cytotoxicity against cancer (PC3 and A375) and MRC5 (normal) cell lines^a. ^aIC₅₀ values are expressed as mean ± SD of three independent experiments.

IC₅₀ values in the range of 76.90–93.07 µg/mL better than the standard cisplatin which showed high toxicity at a concentration of 60.34 µg/mL.

The test results for cytotoxicity and IC₅₀ values of compounds 1–6 treated against PC3 cancer cell lines at different concentrations 5, 15, 25, 50, 75 and 100 µg/mL is presented in Table S2. The cytotoxicity is concentration dependent and all the compounds except for 3 and 6 did not show any significant potency for the inhibition of the cancer cells in the concentration range of 5–50 µg/mL. All the compounds except for 3 did exhibit any significant activity in the concentration range of 5–25 µg/mL for the inhibition of A375 cancer cell lines (Table S3). Based on IC₅₀ values of tested compounds, the order of cytotoxicity is 3 > 6 > 4 > 5 > 2 > 1 and this revealed that hybridisation of 1 with the series of chiral amines played a vital role for the activity. Among the hybrids, the high activity of 3 and 6 could be due to the presence of heterocyclic and lipophilic substituents, respectively, on the Schiff base component of the hybrids. The experiment was repeated three times, with the finding reported as mean ± SD (Figs. S15 and S16).

For a compound to be a potential anticancer drug candidate it must be nontoxic to healthy cell lines. Compounds 1–6 were screened for their toxicity against MRC5 normal cell lines at various concentrations (5–100 µg/

mL) and their test results are depicted in Fig. 4. All the compounds were found to be nontoxic and exhibited cell viability (%) 51–92, at the concentration range of 5–75 $\mu\text{g}/\text{mL}$ better than the standard cisplatin, which showed cell viability (%) 55–80, at the concentration range of 5–50 $\mu\text{g}/\text{mL}$. Therefore, the compounds could be viable potential candidates for the development of new anticancer drugs.

The selectivity index (SI) shown in Table 4, was calculated as the ratio of the IC_{50} for the normal cell line (MRC5) to the IC_{50} for a respective cancerous cell line. Higher values of SI indicate greater anticancer specificity and the compounds displaying SI values higher than 3 were considered to be highly selective⁴⁵. Some of the compounds not only had high cytotoxic activity against cancer cells but also displayed low toxicity against normal (MRC5) cells and their SI values were higher than 3.5. The SI values of compound 3 and 6 in A375 cancer cells were 3.95 and 3.85, respectively. The two compounds have high cytotoxicity to the cancer cells and low cytotoxicity to healthy cell lines. Compounds 3 and 6 were selected as potent compounds for further investigation using computational and molecular docking studies.

DFT study and chemical reactivity parameters

DFT studies were carried out on all the compounds. Their optimized ground state geometries was obtained at the B3LYP-GD3/6–311 + G(d,p) level of theory using Gaussian16 Rev B.01 software. The frontier molecular orbitals, HOMO and LUMO were studied as well as the energy gap between the HOMO–LUMO orbitals which is indicative of the stability and reactivity of these compounds. The HOMO is a region in which electrons can be transferred to unoccupied orbitals, while LUMO is an electron-accepting spot. HOMO was found as bonding orbitals that are dispersed throughout the molecule. Several studies have shown that a lower ΔE HOMO–LUMO corresponds to more bioactivity of a molecule, and this has been used to explain the relative bioactivities of medicinal compounds⁴⁶. Figures 5, 6 and 7 show the HOMO and LUMO of compounds 1, 2, 3, 4, 5 and 6 as

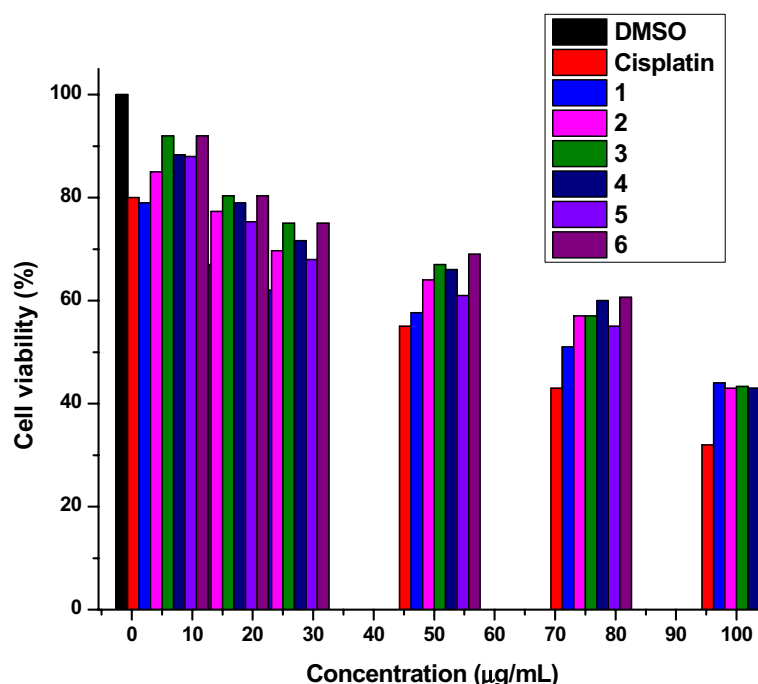


Figure 4. Cell viability (%) of MRC5 normal cell lines treated with various concentrations (5–100 $\mu\text{g}/\text{mL}$) of compounds 1–6 and cisplatin vs cells treated in DMSO (0.1%).

Compound	SI	
	PC3	A375
1	1.02	1.90
2	1.41	2.36
3	2.13	3.95
4	1.59	3.56
5	1.31	2.74
6	2.07	3.85

Table 4. The calculated values of the selectivity index (SI) for compounds 1–6.

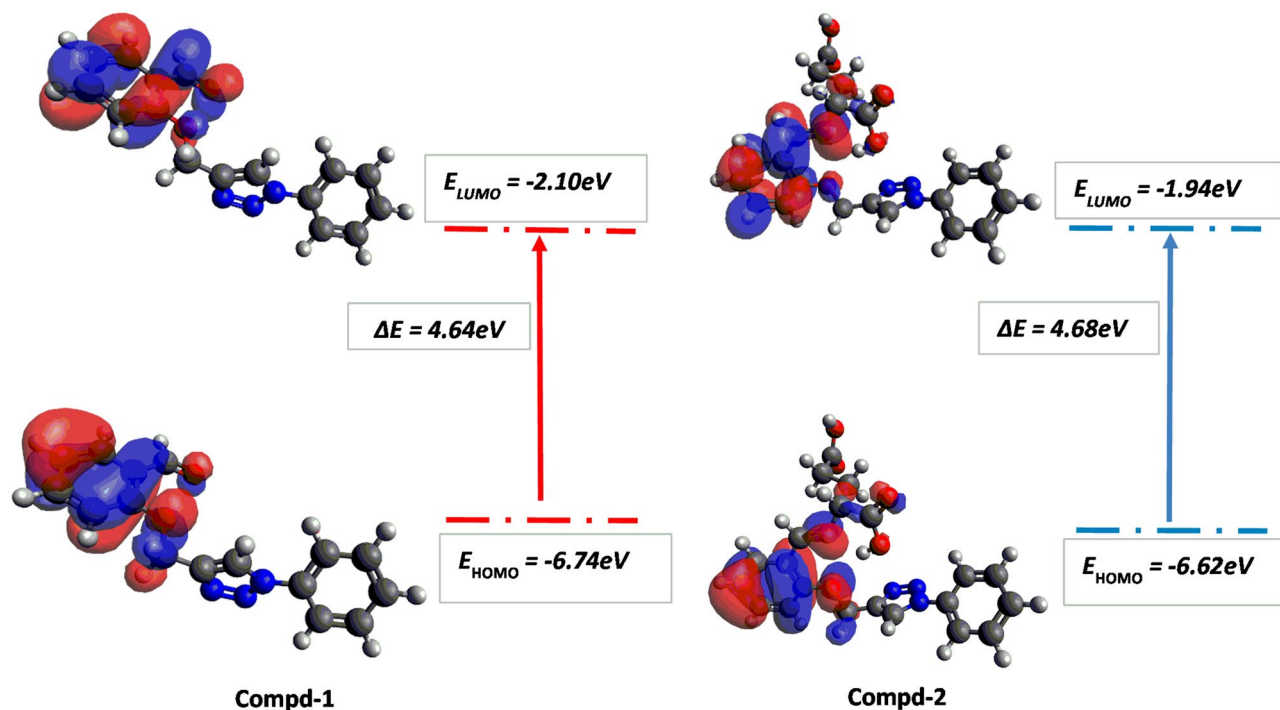


Figure 5. Frontier molecular orbital diagram and energy values for compounds 1 and 2.

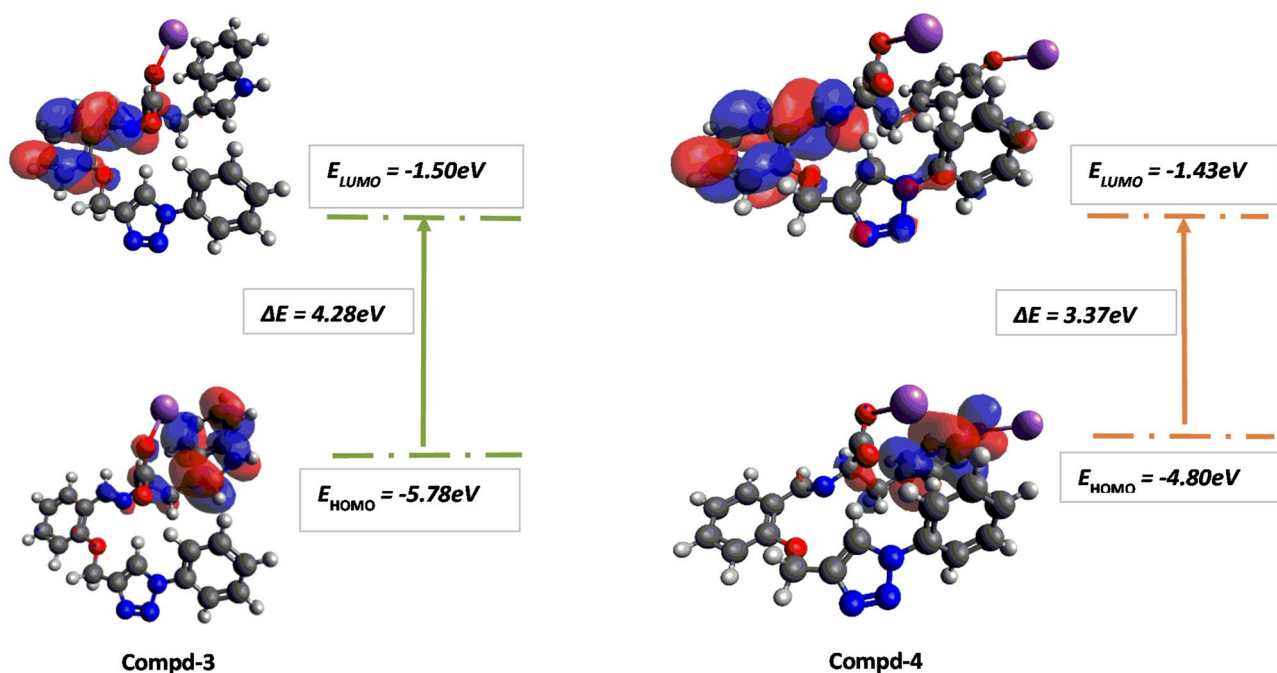


Figure 6. Frontier molecular orbital diagram and energy values for compounds 3 and 4.

well as the energy gap between these frontier orbitals. In all the compounds the HOMO and LUMO are only pronounced on the Schiff base component of the hybrid compound. As shown in Fig. 5, for compound 1 its HOMO and LUMO are evenly distributed over the whole molecule, but the HOMO is more delocalized over the component atoms when compared to its LUMO. In contrast, the main contributions to the HOMO and LUMO of compound 2 are the atoms in its benzene ring and imine moiety. The ΔE HOMO–LUMO for compound 2 is slightly greater than 1 and this is due to the replacement of $-\text{C}(\text{H})=\text{O}$ group from compound 1 by $-\text{C}(\text{H})=\text{N}$ group in compound 2.

Figure 6 shows the HOMO and LUMO for compounds 3 and 4. In both compounds the LUMO is pronounced on the aromatic group from the parent compound and the imine moiety. The HOMO for 3 is distributed on the imine moiety and the tryptophan component, however, in compound 4 the HOMO is delocalized only on the

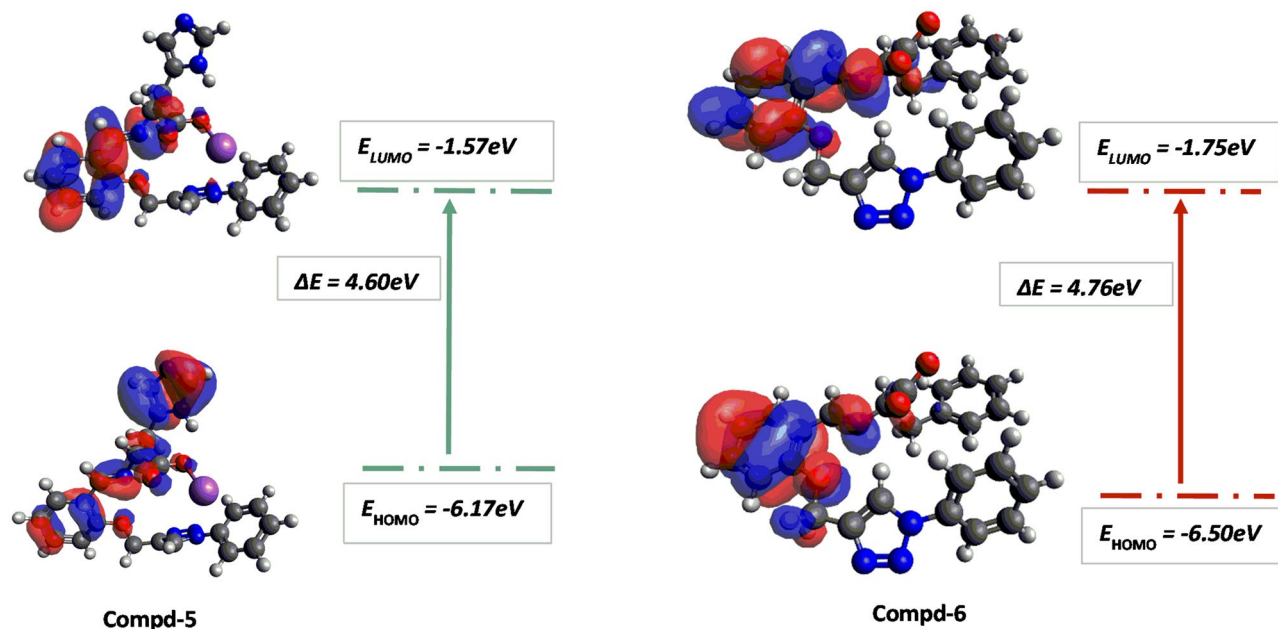


Figure 7. Frontier molecular orbital diagram and energy values for compounds 5 and 6.

aromatic group of the tyrosine component. For compound 4, the ΔE HOMO–LUMO is lower than compound 3 and this is due to the replacement of the tryptophan subunit linked to a sodium ion with a tyrosine subunit linked to two sodium ions.

As shown in Fig. 7, for compound 6 the HOMO and LUMO are evenly distributed on the aromatic group of the parent component and the imine moiety. For compound 5 the HOMO is delocalized over the whole aromatic groups of the Schiff base components (aldehyde and amine sources) and the LUMO is only pronounced on the aromatic group of the parent component and the imine moiety. For compound 5, the ΔE HOMO–LUMO is lower than compound 6 and this is due to the replacement of the phenyl alanine subunit with a histidine subunit linked to a sodium ion.

The ΔE HOMO–LUMO is 4.76, 4.68, 4.64, 4.60, 4.28 and 3.37 eV for compounds 6, 2, 1, 5, 3 and 4 respectively. So, assuming compound 1 is the parent compound, it is observed that the energy gap in compounds 6 and 2 increase slightly due to the replacement of the aldehydic moiety from compound 1 by the imine moiety linked to glutamic acid and phenyl alanine subunit, respectively. For compound 5 decreases slightly due to the replacement of the aldehydic moiety from compound 1 by the imine moiety linked to histidine subunit. The energy gap in compounds 3 and 4 decreases significantly due to the replacement of the aldehyde subunit with an imine moiety linked to tryptophan and tyrosine subunit, respectively.

The Molecular Electrostatic potential (MEP) for compounds 1, 2, 3, 4, 5, and 6 is shown in Fig. 8. MEP indicates the net electrostatic effect exerted at a point in space by the total charge distribution over a molecule. It can be used to study the reactivity of molecules towards electrophilic and nucleophilic reagents as well as their drug-receptor interactions. The different colours on the surfaces (Fig. 8) are indicative of their electrostatic potential values; it increases in the order red < orange < green < blue, where the higher electrostatic potential negative (red) regions of the MEP map are related to electrophilic attack reactivity, whereas the positive (blue) regions are related to nucleophilic attack reactivity, neutral region is represented by green colour. For compound 1, the positive (blue) regions are localized in the oxygen atoms of the carbonyl and ether and on nitrogen atoms of the 1,2,3-triazole ring. The negative (red) regions are found on the aromatic subunit linked to the 1,2,3-triazole component. For compound 2, the negative (red) regions are distributed across most of the components of the molecule and the positive (blue) regions are localized on the two oxygen atoms of the carboxylate and partially on the aromatic subunit linked to the 1,2,3-triazole component. For compounds 3 and 6, the positive (blue) regions are diffused across the whole components of the molecules and the few negative (red) regions are found on the aromatic hydrogen atoms. For compound 4, the positive (blue) regions are found in most of the components of the molecule. The negative (red) regions are localized on the two sodium ions linked to the tyrosine subunit and on the aromatic subunit linked to the 1,2,3-triazole component. For compound 5, the positive (blue) regions are distributed across the Schiff base component of the molecule and the negative (red) regions are localized on the 1,2,3-triazole, aromatic subunit linked to the triazole and on the sodium ion of the carboxylate moiety of histidine subunit. Therefore, the presence of positive (blue) and negative (red) regions on the molecules are evidence for the potential bioactivity of the compounds that could interact through its electrophilic and nucleophilic sites.

Molecular docking analysis

The docking investigation on the studied compounds as Androgen receptor modulators (PDB ID: 5t8e) and Human MIA (PDB ID: 1i1j) inhibitors to down-regulate prostate and skin cancer were executed. The adequate choice of the docking target function impacts the accuracy of the ligand positioning as well as the accuracy of

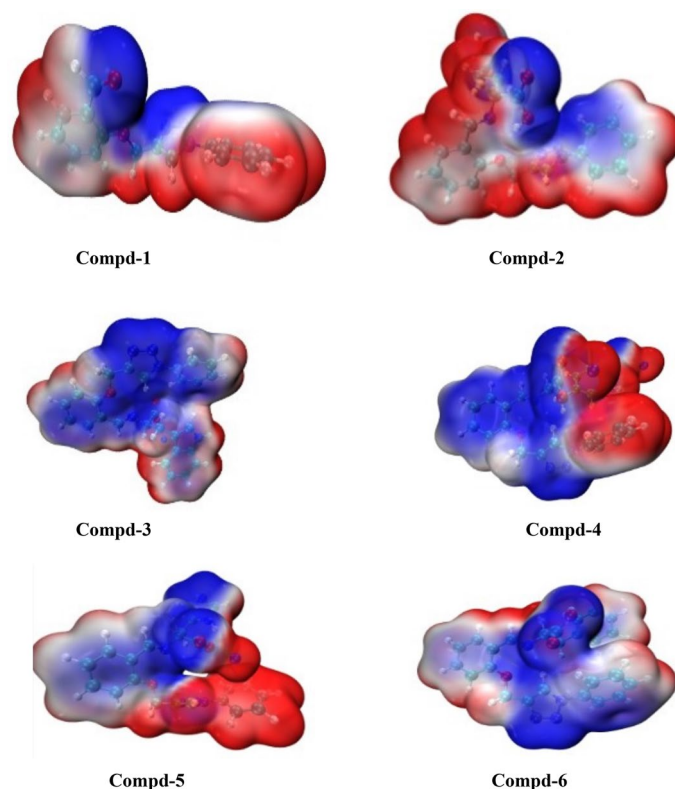


Figure 8. Molecular electrostatic potential maps of compounds 1, 2, 3, 4, 5 and 6.

the protein–ligand binding energy calculation. In this work, the protein structure that is chemically similar to the studied compounds was selected for docking study and before the execution of the docking calculation, the flexibility of the selected protein was evaluated and the proteins with appropriate flexibility were selected for docking study. Also, the method of preparation and resolution ($\leq 2 \text{ \AA}$) of the studied target which agreed with the standard before subjected to further study were considered. The inhibiting activities of the studied synthesized compounds against the studied receptors were compared with the inhibiting activity of Cisplatin against Androgen receptor modulators and Human MIA. As shown in Table 5, the calculated binding affinities for the studied compounds were higher than the reported binding affinity for the referenced compound (Cisplatin). This showed that all the studied compounds proved to be potent in inhibiting Androgen receptor modulators and human MIA than Cisplatin. More so, compound 3 and 6 has proved to be more potent in inhibiting the targets than other studied compounds. This could be confirmed via the combination of amino acid residues and types of biological interactions involved in the docking study between compound 3 and 6 in the active site of Human MIA (PDB ID: 1i1j) complexes and Androgen receptor modulators (PDB ID: 5t8e), respectively. This docking result is in good agreement with the high anticancer activity for compounds 3 and 6 observed in the experimental *in vitro* anticancer study. The type of interactions involved in compound 3—Human MIA complexes and compound 6—Androgen receptor modulators were observed to increase the level of stability and selectivity in the active site of the targets (Figs. 9 and 10).

The calculated binding affinity for compound 1–6 were -6.90 kcal/mol , -6.40 kcal/mol , -6.90 kcal/mol , -7.10 kcal/mol , -8.10 kcal/mol , -8.20 kcal/mol for androgen receptor modulators (PDB ID: 5t8e) while -6.50 kcal/mol , -6.20 kcal/mol , -8.70 kcal/mol , -8.10 kcal/mol , -7.20 kcal/mol , -8.10 kcal/mol for human MIA.

Absorption, distribution, metabolism, and excretion (ADME) prediction

Druglikeness evaluates whether a particular molecule is similar to the known drug or not. It is a complex balance of various properties and structural features of a compound. Lipinski's rule is widely used to determine molecular properties that are important for drug's pharmacokinetic *in vivo*. According to Lipinski's rule of five, a candidate molecule is more likely to be orally active if: (a) $MW \leq 500$, (b) $MLogP \leq 4.15$, (c) $HBD \leq 5$, (d) $HBA \leq 10$, and (e) the number of violations ≤ 1 ⁴⁷. These parameters were calculated by the online available swissADME web tool (<http://www.swissadme.ch/>) and are presented in Table 6. Low molecular weight drug molecules (< 500) are easily transported, diffuse, and absorbed as compared to heavy molecules. The molecular weight of all the compounds were found to be less than 500. Partition coefficient or Log P is an important parameter used in rational drug design to measure molecular hydrophobicity. Hydrophilic/lipophilic nature of drug molecule affects drug absorption, bioavailability, drug-receptor interactions, metabolism of molecules, as well as their toxicity. All the

	Androgen receptor modulators (PDB ID: 5t8e)			Human MIA (PDB ID: 1i1j)		
	Residue involved in the interaction	Type of Interaction involved in the interaction	Binding Affinity (kcal/mol)	Residue involved in the interaction	Type of Interaction involved in the interaction	Binding Affinity (kcal/mol)
1	LEU805, TRP751, THR755, TYR763, VAL684, ARG752	Conventional Hydrogen Bond, Pi-Sigma, Pi-Pi T-Shaped, Pi-Alkyl	- 6.90	PHE49, CYS17, LEU76, ASP103, TYR78, SER50	Conventional Hydrogen Bond, Carbon Hydrogen Bond, Pi-Anion, Pi-Pi Stacked, Alkyl-Alkyl	- 6.50
2	ALA735, LYS905, LYS910, ASP819, TYR739, PRO817, LYS822	Conventional Hydrogen Bond, Pi-Cation, Pi-Anion, Pi-Alkyl	- 6.40	ARG75, ALA73, GLN44, VAL64, THR39, ALA32	Conventional Hydrogen Bond, Pi-Cation, Pi-Sigma, Pi-Alkyl	- 6.20
3	TRP751, GLU681, ASN756	Conventional Hydrogen Bond, Pi-Anion, Pi-Donor Hydrogen Bond	- 6.90	ARG75, CYS106, GLY77, LEU76, TYR78, TRP102	Conventional Hydrogen Bond, carbon hydrogen bond, Pi-Sigma, Pi-Pi Stacked,	- 8.70
4	ARG752, TYR763, TRP751, ASN756, THR755	Conventional Hydrogen Bond, Carbon Hydrogen Bond, Pi-Donor Hydrogen Bond, Pi-Sigma, Pi-Pi T-shaped,	- 7.10	SER50, GLY61, LYS10, ASP103, LEU76, PHE49, SER50	Conventional Hydrogen Bond, Carbon Hydrogen Bond, Pi-Cation, Pi-Sigma, Pi-Pi T-shaped, Pi-Anion	- 8.10
5	ARG752, LYS808, VAL685, TRP718, VAL684, VAL715,	Pi-Cation, Pi-Cation, Pi-Donor Hydrogen Bond, Pi-Sigma, Pi-Pi T-shaped	- 8.10	ASP103, LEU76, TRP102	Carbon Hydrogen Bond, Pi-Sigma, Pi-Pi T-shaped,	- 7.20
6	PRO682, ALA748, ARG752, GLY683, VAL684, ASN756, THR755, TRP751	Conventional Hydrogen Bond, carbon hydrogen bond, Unfavorable Donor-donor, Pi-Cation, Pi-Donor Hydrogen Bond, Amide-Pi Stacked, Pi-Alkyl	- 8.20	TYR78, ASP103, ARG36, LEU76, TRP103	Conventional Hydrogen Bond, carbon hydrogen bond, Pi-Sigma, Pi-Pi T-stacked, Pi-Pi T-shaped, Pi-Alky	- 8.10
Cisplatin	-	-	- 3.87	-	-	- 3.37

Table 5. Calculated binding affinity and interaction involved between the studied complexes.

compounds exhibited MLog P value less than 4.15 which proved the lipophilic efficiency of the compounds. Lipophilicity plays an important role in the distribution of drug after absorption in the body. All the compounds have less than 5 and 10, hydrogen bond donors and acceptors, respectively which obeys the Lipinski's rule of five. Topological polar surface area (TPSA) is closely related to the hydrogen bonding potential of a molecule and is a very good predictor of drug transport properties such as intestinal absorption, bioavailability, blood brain barrier penetration etc⁴⁸. TPSA of all the compounds were found in the range of 87.83–126.90 and it is in the acceptable range of < 160 Å limit. Number of rotatable bonds is a simple topological parameter that measures molecular flexibility and is a good descriptor of oral bioavailability of drugs. The greater the number of rotatable bonds, the more flexible the molecule is to achieve different conformations. The number of rotatable bonds for the compounds were in the range of 9–11. The topological parameter and the number of rotatable bonds are considered to be good descriptors of the oral bioavailability of drugs⁴⁹.

The drug under study is supposed to bind with the biological target. The biological target can be any common protein such as ion channels, enzymes, and receptors. The biological target is also known as the drug target. The predicted bioactivity scores of screened compounds as well as their comparison with the standard drug for GPCR ligand, ion channel modulator, kinase inhibitor, nuclear receptor ligand, protease inhibitor and enzyme inhibitory activity was computed using Molinspiration cheminformatics software (freely available on <https://molinspiration.com>) and are summarized in Table S4. In general, if the bioactivity score (G protein-coupled receptor (GPCR) ligand, a kinase inhibitor, ion channel modulator, nuclear receptor ligand, protease inhibitor, and enzyme inhibitor) of the synthesized compounds is > - 0.5, then the drug is biologically active, but if the score is < - 0.5, then the drug is not active. The bioactivity scores, as provided in Table S4, showed that triazole 1 and the 1,2,3-triazole and chiral Schiff base hybrids 2–6 are active and confirmed their binding flexibilities⁵⁰.

The Swiss ADME software provides a 'BOILED-Egg' visualization (Fig. 11) that displays two important ADME parameters: passive gastrointestinal absorption (HIA) and blood-brain barrier (BBB) access. These parameters mainly use two physicochemical descriptors: the octanol-water partition coefficient (MLogP) and the topological polar surface area (TPSA). In Fig. 11, the egg-shaped categorization plot depicts the white region, which represents the physicochemical space that favours HIA absorption, and the yolk region, which indicates properties that favour BBB permeability. Compounds 1 fall in the yolk region, indicating possible penetration of the BBB. In addition, it is likely that compounds with TPSA < 79 Å² and relatively lipophilic properties reach the central nervous system (CNS). However, the 'BOILED-Egg' approach is limited to passive molecules. The blue dots on the diagram indicate compounds that are likely to be removed from the CNS by p-glycoproteins, while the red dots indicate compounds that are likely to remain in the CNS. Compounds 2–6 exhibit favorable physicochemical properties with low molecular weights and TPSA values < 140 Å², indicating good human intestinal absorption (HIA)⁵¹.

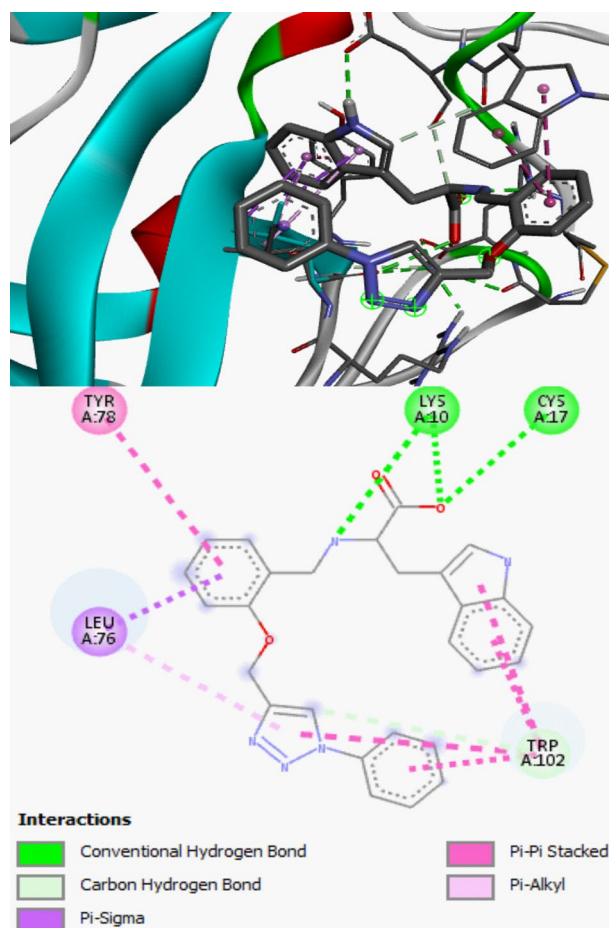


Figure 9. 3D and 2D structure of compound **3** in the active site of human MIA.

Conclusion

The 1,2,3-triazole and chiral Schiff base hybrids **2–6** were successfully synthesized and their chemical structures were established using different spectroscopic techniques. Crystal of compound **1** was obtained and its structure was confirmed by single crystal X-ray diffraction. All compounds were evaluated for their anticancer activity against PC3 prostate cancer, skin cancer and MRC5 normal cells. All the compounds showed significant anticancer activity against the cancerous cells. Among the tested compounds **3** and **6** showed high activity for the inhibition of A375 and PC3 cancer cell lines and low toxicity for the healthy cell lines (MRC5). DFT study on the compounds proved the presence of electrophilic and nucleophilic bioactive sites for receptors. Molecular docking study proved that all the compounds are potent in inhibiting Androgen receptor modulators and human MIA than Cisplatin. The high binding affinity of compounds **3** and **6** plays a vital role for their high anticancer activity observed in the experimental *invitro* anticancer evaluation. Structure activity relationships (SARs) of the tested compounds is in good agreement with DFT and molecular docking studies which proved that the presence of heterocyclic and lipophilic substituent on the Schiff base component of the hybrids is the main factor for high anticancer activity. The compounds exhibited desirable physicochemical properties for druglikeness. Thus, this preliminary study could be a foundation for researchers to gain more understanding on the synthesis and anticancer activity of 1,2,3-triazole and chiral Schiff base hybrids.

Experimental Reagents

All the solvents used were analytical grade. All the reagents were purchased from Sigma Aldrich and were used as received without further purification unless otherwise stated. Salicylaldehyde (97%), potassium carbonate anhydrous (99.5%) (K_2CO_3), acetone ($\geq 99.5\%$), *N,N*-dimethylformamide (DMF, 99.8%), propargyl bromide (80 wt. % in toluene), sodium nitrite ($NaNO_2$, $\geq 97\%$), sodium azide (NaN_3 , $\geq 99.5\%$), copper(II) sulphate pentahydrate ($CuSO_4 \cdot 5H_2O$, 99%), sodium *L*-ascorbate ($\geq 98\%$), sulfuric acid (H_2SO_4 , 98%), *L*-tyrosine ($\geq 99\%$), Phenylalanine ethyl ester hydrochloride ($\geq 99\%$), *L*-tryptophan ($\geq 98\%$), *L*-histidine, *L*-glutamic acid, sodium hydroxide ($NaOH$, $\geq 98\%$), Chloroform-D ($CDCl_3$, 99.8 Atom % D), dimethyl sulfoxide- d_6 (DMSO- d_6 , 99.9 Atom % D).

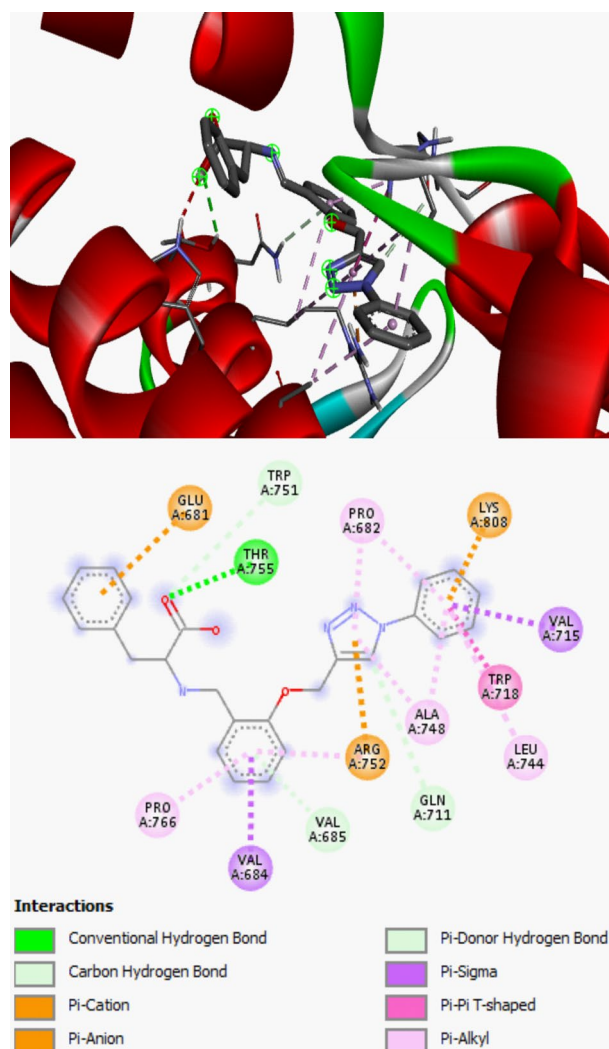


Figure 10. 3D and 2D structure of compound 6 in the active site of Androgen receptor modulators.

Compound	MR ^a	MLogP ^b	TPSA ^c	N _{atoms} ^d	MW ^e	N _{ON} ^f	N _{OHNH} ^g	N _{viol} ^h	N _{roth} ⁱ	Vol ^j
Rule	–	≤ 4.15	–	–	≤ 500	≤ 10	≤ 5	≤ 1	–	–
1	77.73	1.86	57.01	21	279.29	4	0	0	5	248.69
2	108.57	1.32	126.90	17	408.41	8	2	0	10	357.40
3	131.98	2.54	94.39	36	487.49	6	1	0	10	411.24
4	120.75	2.27	87.83	35	486.43	7	0	0	11	387.53
5	112.27	1.03	107.28	32	438.41	7	1	0	10	363.09
6	121.67	2.79	89.60	32	426.47	6	1	0	9	385.00

Table 6. In silico physicochemical data for drug likeness based on the Lipinski rule (SAR). ^aMolar refractivity; ^boctanol-water partition coefficient, calculated by methodology developed by Molinspiration; ^cpolar surface area; ^dnumber of non-hydrogen atoms; ^emolecular weight; ^fnumber of hydrogen-bond acceptor (O and N atoms); ^gnumber of hydrogen-bond donors (OH and NH atoms); ^hnumber of “Rule of five” violations; ⁱnumber of rotatable bonds; ^jmolecular volume.

Instruments and methods

Analytical

Melting points were determined using a Reichert-Jung Thermovar hot-stage microscope and are uncorrected. Infrared spectra were recorded using Tensor 27 Bruker and Perkin Elmer FT-IR spectrum BX. High resolution mass spectra (HRMS) or mass spectra (MS) were carried out on a Waters Synapt G2 instrument at University of Pretoria, South Africa. All ¹H NMR spectra were recorded on Bruker 500 MHz NMR spectrometer at ambient

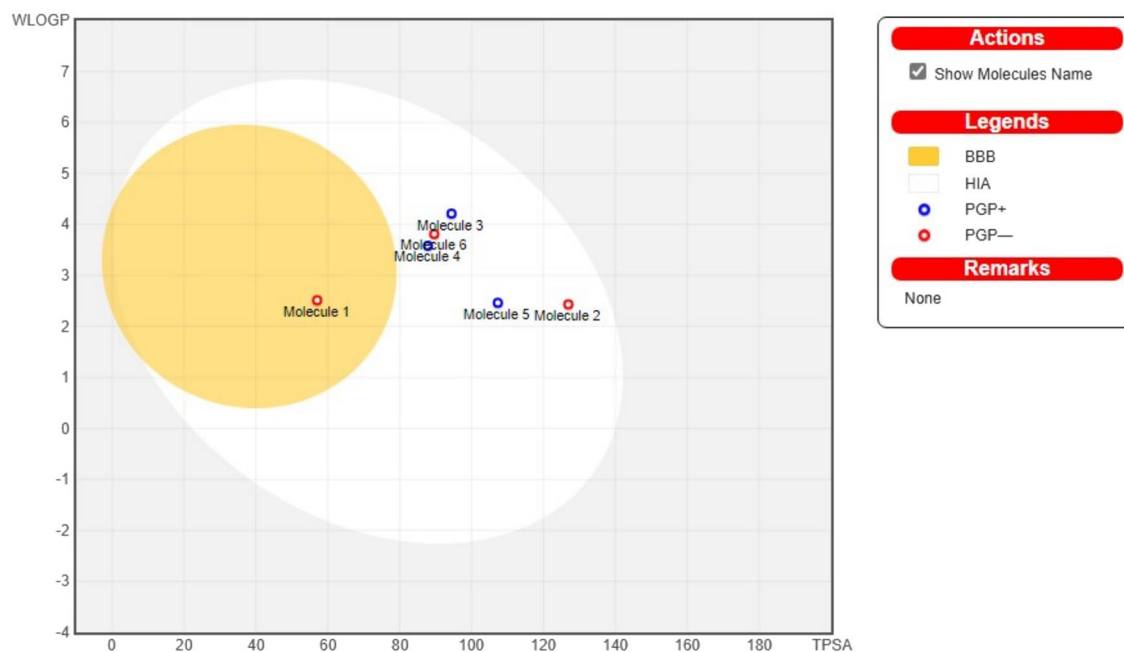


Figure 11. The BOILED-egg visualization predictive model for passive gastrointestinal absorption (hia) and blood–brain barrier (BBB) penetration of compounds 1–6 in the WLOGP-versus-TPSA diagram⁵¹.

temperature and are reported as chemical shift δ in units of parts per million (ppm) with reference to the solvent (2.50 ppm for DMSO- d_6 and 7.26 ppm for C(H)DCl₃) or TMS (0.00 ppm). Multiplicities are presented as: s (singlet); d (doublet); t (triplet); dd (doublet of doublet); and m (multiplet). Coupling constants J values are expressed in Hz and the number of protons expressed as nH. ¹³C NMR spectra were obtained using Bruker 500 MHz NMR spectrometer at ambient temperature. Spectra are reported as chemical shift δ in units of parts per million (ppm) with reference to the deuterated solvent (39.81 ppm for DMSO- d_6 or 77.16 ppm for CDCl₃). The crystal was mounted on a glass fibre and used for the X-ray crystallographic analysis. The X-ray intensity data were collected on a Bruker Apex DUO 4 K CCD diffractometer area detector system, equipped with a graphite monochromator and Mo K α fine-focus sealed tube ($\lambda = 0.71073$ Å) operated at 1.5 KW power (50 kV, 30 mA). The detector was placed at 4 cm from the crystal. Crystal temperature during the data collection was kept constant at 100 (2) K, using an Oxford 700 + series cryostream cooler.

Synthesis

Synthesis of 2-((1-phenyl-1H-1,2,3-triazol-4-yl)methoxy)benzaldehyde (1)

To solution of 2-(prop-2-yn-1-yloxy)benzaldehyde (1.35 g, 8.44 mmol) in DMF: H₂O (100 mL, 4:1) was added azidobenzene (1.21 mL, 10.13 mmol) followed by the addition of CuSO₄·5H₂O (0.0600 mmol, 15.0 mg dissolved in 200 μ L of water) and sodium ascorbate (0.880 mmol, 174 mg dissolved in 800 μ L of water). The reaction mixture was stirred under reflux for 24 h. The hot solution was poured into ice-water mixture, and the precipitate formed was filtered, washed with ice-water (3 \times 25 mL). The solid product was dried *in vacuo* at 100 °C to provide compound 1 as colourless solid. The solid product collected was then recrystallised from ethanol (20 mL, by slow evaporation) and provided compound 5 as crystalline solid⁴⁴. Yield (2.07 g, 7.43 mmol, 88%). m.p.: 147–149 °C. ¹H NMR (500 MHz, CDCl₃, δ): 10.49 (s, 1H, HC=O), 8.08 (s, 1H, H-triazole), 7.84 (d, 1H, $J = 7.8$ Hz, Ar), 7.73 (d, 2H, $J = 7.5$ Hz, Ar), 7.57 (m, 3H), 7.45 (t, 1H, $J = 7.5$ Hz, Ar), 7.21 (t, 1H, $J = 8.5$ Hz, Ar), 7.07 (t, 1H, $J = 7.5$ Hz, Ar), 5.42 (s, 2H, CH₂OAr). ¹³C NMR (126 MHz, CDCl₃, δ): 189.72 (C=O), 160.6 (Ar), 144.4 (N–C=CH), 137.1, 136.2, 130.0, 129.3, 125.5, 121.7, 121.3 (Ar), 120.9 (N–C=CH), 113.3 (Ar), 62.9 (CH₂OAr). FTIR (ν in cm⁻¹): 3150 (w), 3116 (w), 3076 (w), 2956 (w), 2922 (bs), 2796 (w), 2647 (w), 2447 (w), 1961 (w), 1869 (w), 1801 (w), 1675 (s), 1600 (s), 1504 (w), 1481 (m), 1458 (s), 1406 (m), 1338 (w), 1286 (s), 1241 (s), 1189 (m), 1161 (s), 1104 (w), 1046 (s), 989 (m), 903 (w), 846 (m), 823 (s), 754 (s), 686 (s). CHN analysis: Anal. Calcd. for C₁₆H₁₃N₃O₂: C, 68.81%, H, 4.69%, N, 15.05%; Found: C, 68.04%, H, 4.82%, N, 14.71%. ESI-TOF-HRMS: [M + H]⁺ calculated for C₁₆H₁₃N₃O₂: 280.1087, found 280.1091.

General procedure for the synthesis of 1,2,3-triazole and chiral Schiff bases hybrids (2–6)

The reaction was carried out following the literature reported procedure⁵². To a stirred solution of sodium hydroxide (0.043 g, 1.08 mmol) in 20 mL methanol at 80 °C was added two equivalents of the amines. When the combined reaction mixture completely dissolved, compound 1 (0.100 g, 0.358 mmol) was added and the colour of the reaction solution eventually changed to yellow. The reaction was stirred for 1 h at 80 °C. After the solution was cooled down to room temperature 150 mL aliquots of diethyl ether were added. A yellow precipitate appeared. The yellow precipitate was separated from the solution, washed several times with diethyl ether and dried *in vacuo*.

Synthesis of (s,e)-2-((2-((1-phenyl-1H-1,2,3-triazol-4-yl)methoxy)benzylidene)amino)pentanedioic acid (2)

White crystalline solid. Yield (0.121 g, 0.297 mmol, 83%). m.p.: 146–148 °C. ¹H NMR (500 MHz, DMSO-*d*₆, δ) 10.0 (s, 1H, COOH), 10.34 (s, 1H, COOH), 9.00 (s, 1H, HC=N), 7.92 (s, 2H, H-triazole and Ar), 7.70–7.12 (m, 8H, Ar), 5.43 (s, 2H, CH₂OAr), 4.98 (s, 1H, N-CH-CH₂), 3.15 (s, 4H, N-CH-CH₂). ¹³C NMR (126 MHz, DMSO-*d*₆, δ) 189.5 (C=O), 160.4 (C=N), 136.4, 130.0, 128.9, 128.0, 127.7, 122.9, 121.4 (Ar), 120.2 (N-C=CH), 114.3 (Ar), 62.3 (N-CH-CH₂), 56.6 (CH₂OAr), 48.6 (N-CH-CH₂). IR assignments (ν in cm⁻¹): 3479 (s), 3156 (m), 2922 (w), 2879 (w), 1664 (s), 1595 (s), 1507 (m), 1484 (s), 1466 (w), 1455 (s), 1404 (s), 1386 (s), 1335 (m), 1232 (s), 1186 (s), 1158 (s), 1103 (s), 1043 (s), 989 (m), 846 (s), 820 (s), 755 (s), 683 (s), 660 (m), 638 (m). CHN analysis: Anal. Cald. for C₂₁H₂₀N₄O₅: C, 61.76%, H, 4.94%, N, 13.72%; Found: C, 61.08%, H, 5.32%, N, 13.14%.

Synthesis of sodium (s,e)-3-(1H-indol-3-yl)-2-((2-((1-phenyl-1H-1,2,3-triazol-4-yl)methoxy)benzylidene)amino)propanoate (3)

Colourless solid. Yield (0.150 g, 0.308 mmol, 86%). m.p.: 196–198 °C. ¹H NMR: (500 MHz, DMSO-*d*₆, δ) 10.68 (s, 1H, NH), 8.89 (s, 1H, HC=N), 8.31 (s, 1H, H-triazole), 7.90–7.86 (m, 3H, Ar), 7.57 (t, 2H, *J* = 7.20 Hz, Ar), 7.52 (d, 1H, *J* = 8.0 Hz, Ar), 7.46 (t, 1H, *J* = 7.0 Hz, Ar), 7.36 (d, 1H, *J* = 7.5 Hz, Ar), 7.22 (t, 2H, *J* = 8.0 Hz, Ar), 6.99–6.91 (m, 3H, Ar), 6.84 (t, 1H, *J* = 7.2 Hz, Ar), 5.21 (d, 2H, *J* = 8.0 Hz, CH₂OAr), 3.85 (s, 1H, N-CH-CH₂), 3.32 (s, 2H, *J* = 14.0 Hz, N-CH-CH₂). ¹³C NMR (126 MHz, DMSO-*d*₆, δ) 174.8 (C=O), 157.0 (C=N), 154.2 (Ar), 143.9 (N-C=CH), 136.6, 136.0, 131.3, 129.9, 128.8, 127.7, 127.2, 125.2, 123.1, 122.8, 121.0 (Ar), 120.3 (N-C=CH), 118.7, 117.2, 113.4, 113.0, 111.1 (Ar), 78.5 (N-CH-CH₂), 61.9 (CH₂OAr), 30.1 (N-CH-CH₂). IR assignments (ν in cm⁻¹): 3276 (bs), 2367 (w), 1595 (s), 1498 (m), 1435 (s), 1284 (s), 1238 (m), 1166 (m), 1100 (m), 1046 (m), 1000 (m), 878 (m), 832 (m), 755 (s), 689 (s). CHN analysis: Anal. Cald. for C₂₇H₂₂N₅NaO₃: C, 66.52%, H, 4.55%, N, 14.37%; Found: C, 66.13%, H, 4.96%, N, 13.98%.

Synthesis of sodium (s,e)-3-(4-oxidophenyl)-2-((2-((1-phenyl-1H-1,2,3-triazol-4-yl)methoxy)benzylidene)amino)propanoate (4)

Reddish brown coloured solid. Yield (0.135 g, 0.279 mmol, 78%). m.p.: 148–150 °C. ¹H NMR (500 MHz, DMSO-*d*₆, δ) 8.07 (s, 1H, HC=N), 8.01 (s, 1H, H-triazole), 7.94–7.85 (m, 1H, Ar), 7.59 (t, 3H, *J* = 7.5 Hz, Ar), 7.50–7.44 (m, 2H, Ar), 7.36 (t, 1H, *J* = 7.8 Hz, Ar), 7.24 (d, 1H, *J* = 8.5 Hz, Ar), 6.98 (t, 1H, *J* = 7.5 Hz, Ar), 6.45 (d, 2H, *J* = 8.5 Hz, Ar), 5.95 (d, 2H, *J* = 8.0 Hz, Ar), 5.22 (s, 2H, CH₂OAr), 3.56 (d, 1H, *J* = 6.5 Hz, N-CH-CH₂), 2.88 (d, 1H, *J* = 11.0 Hz, N-CH-CH₂), 2.62 (s, 1H, N-CH-CH₂). ¹³C NMR (126 MHz, DMSO-*d*₆, δ) 166.6, 162.4 (Ar), 157.3 (C=N), 144.3 (N-C=CH), 132.1, 129.9, 128.8, 128.1, 127.4, 126.8, 122.8 (Ar), 120.2 (N-C=CH), 113.6 (Ar), 69.8 (N-CH-CH₂), 61.9 (CH₂OAr), 35.8 (N-CH-CH₂). IR assignments (ν in cm⁻¹): 2359 (w), 1598 (s), 1487 (m), 1452 (m), 1375 (m), 1265 (s), 1106 (w), 1046 (m), 1003 (m), 829 (w), 755 (s), 689 (s). CHN analysis: Anal. Cald. for C₂₅H₂₀N₄Na₂O₄: C, 61.73%, H, 4.14%, N, 11.52%; Found: C, 61.34%, H, 4.52%, N, 10.85%.

Synthesis of sodium (s,e)-3-(1 h-indol-3-yl)-2-((2-((1-phenyl-1H-1,2,3-triazol-4-yl)methoxy)benzylidene)amino)propanoate (5)

Brown coloured solid. Yield (0.117 g, 0.268 mmol, 75%). m.p.: 234–236 °C. ¹H NMR (500 MHz, DMSO-*d*₆, δ) 8.06 (s, 1H, HC=N), 8.01 (s, 1H, H-triazole), 7.58 (t, 3H, *J* = 8.0 Hz, Ar), 7.47–7.43 (m, 2H, Ar), 7.33 (d, 1H, *J* = 7.5 Hz, Ar), 7.10–7.02 (m, 3H, Ar), 6.88–6.66 (m, 2H, Ar), 5.40 (s, 2H, CH₂OAr), 2.68 (s, 2H, N-CH-CH₂), 2.63 (d, 2H, *J* = 11.0 Hz, N-CH-CH₂). ¹³C NMR (126 MHz, DMSO-*d*₆, δ) 192.1 (C=O), 137.0, 131.8, 130.4, 130.0, 129.1, 128.1, 125.7, 123.7, 100.9 (Ar), 59.7 (N-CH-CH₂), 58.1 (CH₂OAr), 55.5 (N-CH-CH₂). IR assignments (ν in cm⁻¹): 3245 (bs), 1584 (s), 1487 (w), 1449 (w), 1406 (s), 1341 (w), 1289 (w), 1224 (s), 1101 (w), 1046 (m), 1000 (w), 881 (m), 815 (m), 755 (s), 689 (s). CHN analysis: Anal. Cald. for C₂₂H₁₉N₆NaO₃: C, 60.27%, H, 4.37%, N, 19.17%; Found: C, 59.61%, H, 4.79%, N, 18.58%.

Synthesis of (e)-3-phenyl-2-((2-((1-phenyl-1H-1,2,3-triazol-4-yl)methoxy)benzylidene)amino)propanoic acid (6)

Phenylalanine ethyl ester hydrochloride (0.205 g, 0.358 mmol) was dissolved in ethanol and compound **1** (0.100 g, 0.358 mmol) was added to this solution. Sodium hydroxide solution (50% in water) was prepared and added to the solution to proceed the reaction in basic condition. The reaction mixture was refluxed at 50 °C for 7 h. The solution was cooled, and solvent was removed by rotary evaporator. The product was filtered, the precipitated product was washed with ethanol and dried. White crystalline solid. Yield (0.130 g, 0.304 mmol, 85%). m.p.: 230–232 °C. ¹H NMR (500 MHz, DMSO-*d*₆, δ) 10.42 (s, 1H, COOH), 9.02 (s, 1H, HC=N), 8.92 (s, 1H, H-triazole), 7.91 (t, 2H, *J* = 8.2 Hz, Ar), 7.72–7.67 (m, 2H, Ar), 7.60 (t, 2H, *J* = 7.2 Hz, Ar), 7.51–7.46 (m, 3H, Ar), 7.39 (d, 1H, *J* = 7.5 Hz, Ar), 7.34 (t, 1H, *J* = 7.0 Hz, Ar), 7.27 (d, 1H, *J* = 8.0 Hz, Ar), 7.12 (t, 1H, *J* = 7.2 Hz, Ar), 6.98 (t, 1H, *J* = 7.5 Hz, Ar), 5.55 (s, 1H, N-CH-CH₂), 5.44 (s, 2H, CH₂OAr), 5.26 (s, 2H, N-CH-CH₂). ¹³C NMR (126 MHz, DMSO-*d*₆, δ) 189.3 (C=O), 160.3 (C=N), 155.5 (Ar), 143.6 (N-C=CH), 136.5, 129.8, 127.6, 126.9, 124.6, 122.7, 121.2, 120.5 (Ar), 120.1 (N-C=CH), 114.2, 113.0 (Ar), 98.6 (N-CH-CH₂), 62.2 (CH₂OAr), 53.4 (N-CH-CH₂). IR assignments (ν in cm⁻¹): 3285 (bs), 3062 (w), 3027 (w), 2927 (w), 2358 (w), 1578 (s), 1489 (w), 1449 (w), 1409 (s), 1341 (m), 1238 (m), 1189 (w), 1158 (w), 1098 (w), 1078 (w), 1032 (m), 900 (m), 862 (m), 755 (s), 697 (s). CHN analysis: Anal. Cald. for C₂₅H₂₂N₄O₃: C, 70.41%, H, 5.20%, N, 13.14%; Found: C, 69.75%, H, 5.59%, N, 12.52%.

Anticancer and cytotoxicity evaluation*Cell culture*

PC3, A375, and MRC5 cell lines were purchased from ATCC and were cultured in Dulbecco's Modified Eagle Media (DMEM) supplemented with 10% Fetal Bovine Serum (FBS) (Highveld biological), 1% gentamycin and 1% penicillin/streptomycin (Sigma, USA). Cells were maintained at 37 °C under 5% of carbon dioxide (CO₂)

and 95% relative humidity. The cells were trypsinized (0.1% trypsin) once reached 85% confluency and counted, plated in 96 well plates for treatment with various concentrations of the compounds 1–6.

Assay background

The growth inhibitory effect and cytotoxicity of the compounds were tested in triplicate against two cancer cell lines (PC3 and A375) and one healthy cell line (MRC5), respectively using Alamar Blue assay.

AlamarBlue assay

PC3, A375, and MRC5 cell lines were cultured in 96 well tissue culture plates. A cell density of 2.5×10^4 cells in 90 μL of media per well was added to the plates and incubated overnight before treatment with a range of concentrations (5–100 $\mu\text{g}/\text{mL}$) of compounds 1–6. The controls of the experiment were DMEM only (blank), cells treated with DMSO (0.1%), untreated cells in DMEM, and 100 μM cisplatin (Sigma Aldrich) (positive control). Cells were treated for 24 h. 10 μL of AlamarBlue (Thermo Fisher Scientific) was added to each well at 22 h after treatment and incubated for 2 h at 37 °C in the dark since AlamarBlue is light sensitive. Cell viability was measured using AlamarBlue and readings were obtained in terms of fluorescent values using a microplate reader (BioTek Synergy HT). Samples were exposed to an excitation wavelength of 530 nm and at the emission wavelength of 590 nm. Cell viability percentage was calculated using the formula below:

$$\text{Cell viability} = \frac{\text{absorbance of treated cells} - \text{absorbance of blank}}{\text{absorbance of untreated cells} - \text{absorbance of blank}} \times 100\%$$

Computational method

The Gauss View 5.0⁵³ molecular builder and visualization software was used to construct input structures of Compounds 1–6. Geometry optimization of these structures was then executed at the B3LYP-gD3/6–311++G(d,p) level of theory using Gaussian 16 Rev B.01 software⁵⁴. The solvation environment was modelled with the default Polarizable Continuum Model (PCM) in Gaussian using methanol as solvent. Frequency calculations were carried out using the harmonic rotor approximation as implemented in Gaussian software. The absence of imaginary vibrational frequencies in the optimized structures confirmed them as true representative ground state structures of the compounds under investigation. Gauss View 5.0 software was subsequently used to generate and visualize the dipole moment vectors and output representations for the investigated compounds. Molecular Electrostatic Potential (MEP) map was generated using multiwfn software version 3.8^{55,56} while the Frontier Orbital energy plots and diagrams were obtained using Avogadro software⁵⁷.

Molecular docking study

The interactions between the studied compounds and Androgen receptor modulators (PDB ID: 5t8e)⁵⁸ for prostate cancer as well as Human MIA (PDB ID: 1i1j)⁵⁹ for skin cancer were investigated using molecular docking study. The study was executed using appropriate software such as Spartan 14 software⁶⁰, Pymol v 1.7.4 software⁶¹, AutoDockTools-1.5.6⁶², Autodock vina software⁶³ and discovery studio client v19.1.0.18287⁶⁴. The studied compounds (1–6) were optimized using 6-31G* in order to obtain full geometry before subjecting to docking software. The optimized compounds were converted to .pdb format from spartan format using Spartan 14 software which was further converted to .pdbqt using AutoDockTools-1.5.6. The studied receptors were retrieved from online protein database (<https://www.rcsb.org/>) and treated by removing small molecules as well as water molecules downloaded with the studied receptors using discovery studio client v19.1.0.18287. The docking of the studied compounds against the target requires locating the active site in the treated protein; therefore, the calculated value for the centre and size in X, Y and Z directions that show the located binding site were 20.163, 5.238, and 10.845 for the centre and 72, 62 and 74 for size (Androgen receptor modulators (PDB ID: 5t8e)) while 20.003, 21.173 and 1.583 for the center and 48, 50 and 40 for size described the active site of the Human MIA (PDB ID: 1i1j). The binding affinities for the studied complexes were accomplished using Autodock vina software before post-docking analysis.

Accession codes

CCDC 2297996 contains the supplementary crystallographic data for this paper. These data can be obtained free of charge via www.ccdc.cam.ac.uk/data_request/cif, or by emailing data_request@ccdc.cam.ac.uk, or by contacting The Cambridge Crystallographic Data Centre, 12 Union Road, Cambridge CB2 1EZ, UK; fax: +44 1223 336 033.

Data availability

All the findings are available in the manuscript and the supplementary material.

Received: 4 January 2024; Accepted: 20 March 2024

Published online: 23 March 2024

References

- Çot, A. *et al.* Synthesis, characterization, antioxidant and anticancer activity of new hybrid structures based on diarylmethanol and 1,2,3-triazole. *J. Mol. Struct.* **1269**, 133763 (2022).
- Popova, E. A., Protas, A. V. & Trifonov, R. E. Tetrazole derivatives as promising anticancer agents. *Anticancer Agents Med. Chem.* **17**, 1856–1868 (2017).

3. Sung, H. *et al.* Global cancer statistics 2020: GLOBOCAN estimates of incidence and mortality worldwide for 36 cancers in 185 countries. *CA Cancer J. Clin.* **71**, 209–249 (2021).
4. Philip, C. C., Mathew, A. & John, M. J. Cancer care: Challenges in the developing world. *Cancer Res. Treat.* **1**, 58–62 (2018).
5. Strzelecka, M., Wiatrak, B., Jawien, P., Czynnikowska, Z. & Swiątek, P. New Schiff bases derived from dimethylpyridine-1,2,4-triazole hybrid as cytotoxic agents targeting gastrointestinal cancers: Design, synthesis, biological evaluation and molecular docking studies. *Bio. Organic. Chem.* **139**, 106758 (2023).
6. Hassan, H. M. *et al.* Synthesis and biological evaluation of novel triazolyl 4-anilinoquinazolines as anticancer agents. *Med. Chem. Res.* **28**, 1766–1772 (2019).
7. Decker, M. Hybrid molecules incorporating natural products: Applications in cancer therapy, neurodegenerative disorders and beyond. *Curr. Med. Chem.* **18**, 1464–1475 (2011).
8. Kerru, N., Singh, P., Koorbanally, N., Raj, R. & Kumar, V. Recent advances (2015–2016) in anticancer hybrids. *Eur. J. Med. Chem.* **142**, 179–212 (2017).
9. Szumilak, M., Wiktorowska-Owczarek, A. & Stanczak, A. Hybrid drugs—A strategy for overcoming anticancer drug resistance?. *Molecules* **26**(9), 2601 (2021).
10. Fedorowicz, J. & Saczewski, J. Modifications of quinolones and fluoroquinolones: hybrid compounds and dual-action molecules. *Monatshefte für Chemie Chem. Mon.* **149**, 1199–1245 (2018).
11. Zhang, B. Comprehensive review on the anti-bacterial activity of 1,2,3-triazole. *Eur. J. Med. Chem.* **168**, 357–372 (2019).
12. Naveen, A. *et al.* Synthesis, molecular docking and DFT studies on biologically active 1,4-disubstituted-1,2,3-triazole-semicarbazone hybrid molecules. *New J. Chem.* **43**(21), 8052–8058 (2019).
13. Shiri, P., Ramezanzpour, S., Amani, A. M. & Dehaen, W. A patent review on efficient strategies for the total synthesis of pazopanib, regorafenib and lenvatinib as novel anti-angiogenesis receptor tyrosine kinase inhibitors for cancer therapy. *Mol. Divers.* **26**(5), 2981–3002 (2022).
14. Mashayekh, K. & Shiri, P. An overview of recent advances in the applications of click chemistry in the synthesis of bioconjugates with anticancer activities. *ChemistrySelect* **4**(46), 13459–13478 (2019).
15. Singu, P. S. *et al.* Benzimidazole-1,2,3-triazole hybrid molecules: Synthesis and study of their interaction with G-quadruplex DNA. *RSC. Med. Chem.* **12**(3), 416–429 (2021).
16. Singh, A. K. *et al.* Concept of hybrid drugs and recent advancements in anticancer hybrids. *Pharmaceuticals* **15**(9), 1071 (2022).
17. Bonandi, E. *et al.* The 1,2,3-triazole ring as a bioisostere in medicinal chemistry. *Drug. Discov. Today* **22**(10), 1572–1581 (2017).
18. Boratynski, P. J. *et al.* Triazole biheterocycles from cinchona alkaloids: Coordination and antiproliferative properties. *ChemistrySelect* **3**(32), 9368–9373 (2018).
19. Xu, Z. 1,2,3-Triazole-containing hybrids with potential antibacterial activity against methicillin-resistant *Staphylococcus aureus* (MRSA). *Eur. J. Med. Chem.* **206**, 112686 (2020).
20. Naveen, *et al.* Design, synthesis, biological activity, molecular docking and computational studies on novel 1,4-disubstituted-1,2,3-Triazole-Thiosemicarbazone hybrid molecules. *J. Mol. Struct.* **1209**, 127951 (2020).
21. Chu, X.-M. *et al.* Triazole derivatives and their antiparasitic and antimalarial activities. *Eur. J. Med. Chem.* **166**, 206–223 (2019).
22. Feng, L. S. *et al.* Hybrid molecules with potential in vitro antiparasitic and in vivo antimalarial activity against drug-resistant *Plasmodium falciparum*. *Med. Res. Rev.* **40**, 931–971 (2020).
23. Rani, A. *et al.* CuAAC ensembled 1,2,3-triazole-linked isosteres as pharmacophores in drug discovery: Review. *RSC. Adv.* **10**, 5610–5635 (2020).
24. Nehra, N., Tittal, R. K., Vikas, D. G., Naveen, & Lal, K. Synthesis, antifungal studies, molecular docking, ADME and DNA interaction studies of 4-hydroxyphenyl benzothiazole linked 1,2,3-triazoles. *J. Mol. Struct.* **1245**, 131013 (2021).
25. Feng, L. S., Zheng, M. J., Zhao, F. & Liu, D. 1,2,3-triazole hybrids with Anti-HIV-1 activity. *Arch. Pharm.* **354**(1), 2000163 (2021).
26. Zhang, S. *et al.* Triazole derivatives and their anti-tubercular activity. *Eur. J. Med. Chem.* **138**, 501–513 (2017).
27. Yan, M. *et al.* Opportunities and challenges of using five-membered ring compounds as promising antitubercular agents. *Drug. Dev. Res.* **81**(4), 402–418 (2020).
28. Lal, K. & Yadav, P. Recent advancements in 1, 4-disubstituted 1h–1,2,3-triazoles as potential anticancer agents. *Anti-Cancer Agents Med. Chem.* **18**(1), 26–37 (2018).
29. Slavova, K. I., Todorov, L. T., Belskaya, N. P., Palafox, M. A. & Kostova, I. P. Developments in the application of 1,2,3-triazoles in cancer treatment. *Recent Pat. Anticancer Drug. Discov.* **15**(2), 92–112 (2020).
30. Yadav, P. *et al.* Green synthesis and anticancer potential of chalcone linked-1,2,3-triazoles. *Eur. J. Med. Chem.* **126**, 944–953 (2017).
31. Kumar, S., Lal, B. & Tittal, R. K. Green synthesis of 1,4-disubstituted 1,2,3-triazoles: A sustainable approach. *Green Chem.* **26**, 1725–1769 (2024).
32. Liang, T., Sun, X., Li, W., Hou, G. & Gao, F. 1,2,3-triazole-containing compounds as anti-lung cancer agents: current developments, mechanisms of action, and structure-activity relationship. *Front. Pharmacol.* **12**, 661173 (2022).
33. Ashram, M., Habashneh, A. Y., Bardawel, S. & Taha, M. O. A Click synthesis, molecular docking and biological evaluation of 1,2,3-triazoles-benzoxazepine hybrid as potential anticancer agents. *Med. Chem. Res.* **32**(2), 271–287 (2023).
34. Boulechfar, C. *et al.* Schiff bases and their metal Complexes: A review on the history, synthesis, and applications. *Inorg. Chem. Commun.* **150**, 110451 (2023).
35. Dzeikala, A. & Sykula, A. Schiff bases as important class of pharmacological agents. *J. Pharm. Pharmacol.* **6**, 989–1009 (2018).
36. Noser, A. A., Abdelmonsef, A. H., El-Naggar, M. & Salem, M. M. New amino acid schiff bases as anticancer agents via potential mitochondrial complex I-associated hexokinase inhibition and targeting AMP-protein kinases/mTOR signaling pathway. *Molecules* **26**, 5332 (2021).
37. Uddin, N. *et al.* Synthesis, characterization, and anticancer activity of Schiff bases. *J. Biomol. Struct. Dyn.* **38**, 3246–3259 (2020).
38. Sadia, M. *et al.* Schiff base ligand L synthesis and its evaluation as anticancer and antidepressant agent. *J. King Saud. Univ. Sci.* **33**, 101331 (2021).
39. Zhou, X.-Q. *et al.* Copper complexes based on chiral Schiff-base ligands: DNA/BSA binding ability, DNA cleavage activity, cytotoxicity and mechanism of apoptosis. *Eur. J. Med. Chem.* **14**, 244–256 (2016).
40. Kar, K., Ghosh, D., Kabi, B. & Chandra, A. A. concise review on cobalt Schiff base complexes as anticancer agents. *Polyhedron* **222**, 115890 (2022).
41. Catalano, A. *et al.* A review on the advancements in the field of metal complexes with schiff bases as antiproliferative agents. *Appl. Sci.* **11**, 6027 (2021).
42. Tabassum, S. *et al.* Chiral heterobimetallic complexes targeting human DNA-topoisomerase Ia. *Dalton Trans.* **42**, 16749–16761 (2013).
43. Jana, A. *et al.* Evaluation of the anticancer activities with various ligand substituents in Co(II/III)-picolyl phenolate derivatives: synthesis, characterization, DFT, DNA cleavage, and molecular docking studies. *Dalton Trans.* **51**, 2346–2363 (2022).
44. Belay, Y. *et al.* Molecular hybrid of 1,2,3-triazole and schiff base as potential antibacterial agents: DFT, molecular docking and ADME studies. *J. Mol. Struct.* **1286**, 135617 (2023).
45. Wu, X. L. *et al.* Antitumor activity and mechanism study of riluzole and its derivatives. *I. J. P. R.* **19**, 217–230 (2020).
46. Swislocka, R., Regulska, E., Karpinska, J., Swiderski, G. & Lewandowski, W. Molecular structure and antioxidant properties of alkali metal salts of rosmarinic acid. experimental and DFT studies. *Molecules* **24**, 2645–2667 (2019).

47. Lipinski, C. A., Lombardo, F., Dominy, B. W. & Feeney, P. J. Experimental and computational approaches to estimate solubility and permeability in drug discovery and development settings. *Adv. Drug Delivery Rev.* **46**, 3–26 (2001).
48. Veber, D. F. *et al.* Molecular properties that influence the oral bioavailability of drug candidates. *J. Med. Chem.* **45**, 2615–2623 (2002).
49. Nehra, N., Tittal, R. K. & Ghule, V. D. 1,2,3-triazoles of 8-hydroxyquinoline and HBT: Synthesis and Studies (DNA binding, antimicrobial, molecular docking, ADME, and DFT). *ACS Omega* **6**, 27089–27100 (2021).
50. Sharma, K., Tittal, R. K., Lal, K., Mathpati, R. S. & Ghule, V. D. Fluorescent 7-azaindole N-linked 1,2,3-triazole: Synthesis and study of antimicrobial, molecular docking, ADME and DFT properties. *N. J. Chem.* **47**, 9077–9086 (2023).
51. Khatoon, H., Malek, E. A., Faudzi, S. M. & Rukayadi, Y. Synthesis of a series of quinoxaline derivatives and their antibacterial effectiveness against pathogenic bacteria. *Chem. Select* **9**, e202305073 (2024).
52. Pervaiz, M. *et al.* Synthesis, spectral and antimicrobial studies of amino acid derivative Schiff base metal (Co, Mn, Cu, and Cd) complexes. *Spectrochim. Acta A Mol. Biomol. Spectrosc.* **206**, 642–649 (2019).
53. Dennington, R., Keith, T. A. & Millam, J. M. GaussView, Version 5.0 (Semichem Inc., Shawnee Mission, KS, 2016).
54. Frisch, M. J. *et al.* Gaussian 16, Revision B.01 (Gaussian, Inc., Wallingford CT, 2016).
55. Lu, T. & Chen, F. Multiwfn: A multifunctional wavefunction analyzer. *J. Comput. Chem.* **33**, 580–592 (2012).
56. Zhang, J. & Lu, T. Efficient evaluation of electrostatic potential with computerized optimized code. *Phys. Chem. Chem. Phys.* **23**, 20323–20328 (2021).
57. Avogadro: An open-source molecular builder and visualization tool. Version 1.2.0. <http://avogadro.cc/>.
58. Asano, M. *et al.* Synthesis and biological evaluation of novel selective androgen receptor modulators (SARMs). Part II: Optimization of 4-(pyrrolidin-1-yl)benzotrile derivatives. *Bioorg. Med. Chem. Lett.* **27**, 1897–1901 (2017).
59. Lougheed, J. C., Holton, J. M., Alber, T., Bazan, J. F. & Handel, T. M. Structure of melanoma inhibitory activity protein, a member of a recently identified family of secreted proteins. *P. N. A. S.* **98**, 5515–5520 (2001).
60. Oyebamiji, A. K., Fadare, O. A. & Semire, B. Hybrid-based drug design of 1,2,3-triazolepyrimidine-hybrid derivatives: Efficient inhibiting agents of mesenchymal–epithelial transition factor reducing gastric cancer cell growth. *J. Chem. Res.* **44**, 277–280 (2020).
61. Abdul-Hammed, M., Semire, B., Adegboye, S. A., Oyebamiji, A. K. & Olowolafe, T. A. Inhibition of cyclooxygenase-2 and thymidylate synthase by dietary sphingomyelins: Insights from DFT and molecular docking studies. *Phys. Chem. Res.* **8**, 296–310 (2020).
62. Oyewole, R. O., Oyebamiji, A. K. & Semire, B. Theoretical calculations of molecular descriptors for anticancer activities of 1,2,3-triazole-pyrimidine derivatives against gastric cancer cell line (MGC-803): DFT, QSAR and docking approaches. *Heliyon* **6**(5), e03926 (2020).
63. Adegoke, R. O., Oyebamiji, A. K. & Semire, B. Dataset on the DFT-QSAR, and docking approaches for anticancer activities of 1, 2, 3-triazole-pyrimidine derivatives against Human Esophageal Carcinoma (EC-109). *Data Brief.* **31**, 105963 (2020).
64. OKE, A. M. *et al.* Inhibition of angiotensin converting enzyme by phytochemicals in Cucurbita pepo L.: In silico approach, pharmacological research-modern Chinese medicine **4**, 100142 (2022).

Acknowledgements

The authors acknowledge the Department of Biochemistry of the University of Johannesburg for cytotoxicity test of the compounds. The Centre for high performance computing (CHPC), South Africa, for providing computational resources for this research project. The Department of Chemical Sciences of the University of Johannesburg is also recognized for providing laboratory space, chemicals, and equipment to facilitate this work.

Author contributions

YB: conceptualization, methodology and writing; AM: review, editing and supervision; FM: perform experiment; AO: molecular docking study; AA: DFT computational Study; LM: cytotoxicity evaluation.

Funding

This research did not receive any specific grant from funding agencies in the public, commercial, or not-for-profit sectors.

Competing interests

The authors declare no competing interests.

Additional information

Supplementary Information The online version contains supplementary material available at <https://doi.org/10.1038/s41598-024-57689-5>.

Correspondence and requests for materials should be addressed to Y.B.

Reprints and permissions information is available at www.nature.com/reprints.

Publisher's note Springer Nature remains neutral with regard to jurisdictional claims in published maps and institutional affiliations.



Open Access This article is licensed under a Creative Commons Attribution 4.0 International License, which permits use, sharing, adaptation, distribution and reproduction in any medium or format, as long as you give appropriate credit to the original author(s) and the source, provide a link to the Creative Commons licence, and indicate if changes were made. The images or other third party material in this article are included in the article's Creative Commons licence, unless indicated otherwise in a credit line to the material. If material is not included in the article's Creative Commons licence and your intended use is not permitted by statutory regulation or exceeds the permitted use, you will need to obtain permission directly from the copyright holder. To view a copy of this licence, visit <http://creativecommons.org/licenses/by/4.0/>.

© The Author(s) 2024